

Experimental demonstration of information to energy conversion in a quantum system at the Landauer Limit

John P. P. Silva, Roberto S. Sarthour, Alexandre M. Souza, and Ivan S. Oliveira
Centro Brasileiro de Pesquisas Físicas, Rua Dr. Xavier Sigaud 150, 22290-180 Rio de Janeiro, Brazil

John Goold
*The Abdus Salam International Centre for Theoretical Physics (ICTP), Trieste, Italy**

Kavan Modi
School of Physics, Monash University, Victoria 3800, Australia

Diogo O. Soares-Pinto
*Instituto de Física de São Carlos, Universidade de São Paulo,
POBox 369, 13560-970 São Carlos, São Paulo, Brazi*

Lucas C. Céleri
Instituto de Física, Universidade Federal de Goiás, Caixa Postal 131 74001-970, Goiânia, Brazil†

In 1961, Rolf Landauer demonstrated a revolutionary principle which provided a definitive link between the mathematical theory of information and the physical theory of thermodynamics [1]. Landauer’s principle states that in any irreversible computation there is an unavoidable entropy production, manifested as heat, dissipated to the non-information bearing degrees of freedom of the computer. Landauer found that this dissipated heat is bounded from below by the information theoretic entropy change. Some years later Charles Bennett [2] and independently Oliver Penrose [3], used this principle to explain how to resolve the long standing Maxwell’s demon problem in thermodynamics. The demon as first conceived by Maxwell [4] and named by Kelvin [5], has had an infamous and often controversial history which spans the entire development of statistical mechanics [6–8]. Controversies and philosophical issues aside, both the demon and Landauer’s principle have, at their core, simple but pragmatic applications. Landauer’s principle sets fundamental thermodynamic constraints for (classical and quantum) information processing. Here we employ a nuclear magnetic resonance setup to measure the heat dissipated in elementary quantum logic gates at the Landauer limit. This allows for the detailed study of entropy production in quantum information processors.

Almost half a century has passed and the Landauer limit has finally been reached in several experiments on classical platforms [9–13]. This delay is due to the fundamental difficulty of dealing with systems of only a few degrees of freedom, where the fluctuations about average behaviour are dominant. For these systems the concept of large numbers and hence any notion of thermodynamic equilibrium does not hold. However, the past 20 years has seen a rapid progress in

non-equilibrium statistical mechanics with the development of stochastic thermodynamics [14] and the associated discovery of various fluctuation theorems [15]. Within this framework, thermodynamic quantities such as heat, work, and entropy now become stochastic variables described by appropriate probability distributions over individual phase space trajectories. This approach not only allows physicists to explore the ultimate thermodynamic limits of microscopic systems but also their information processing capabilities [9–13].

Turning towards quantum systems, a picture of non-equilibrium thermodynamics has also emerged with thermodynamic quantities such as heat, work and entropy being formulated as stochastic variables [16, 17]. As expected, in the quantum domain, the situation is more delicate. The absence of a phase space picture due to intrinsic quantum uncertainty aside, one also has to cope with the necessity of performing invasive projective measurements on to a time dependent energy eigenbasis [18]. Until recently, this restrictive necessity has hindered experimental advances in studying the non-equilibrium thermodynamics of quantum systems. However, recent proposals have outlined that the quantum work distribution maybe extracted without the need of performing these measurements in favour of implementing phase estimation of an appropriately coupled ancilla [19, 20] which samples the characteristic function of the distribution of the thermodynamic quantity. These schemes were recently realised experimentally and allowed for the verification of the quantum work fluctuation relations on a Nuclear Magnetic Resonance (NMR) system [21].

The phase estimation schemes for extraction of work statistics [19, 20], have been specifically tailored towards driven quantum systems undergoing a unitary dynamics. Since their inception, interesting extensions have been made in order to explore the thermodynamic fluctuations of open systems [22–24]. In [24] it was shown how the original schemes [19, 20] are modified in order to extract the distribution of heat dissipated to a reservoir in a generic unitary process on a system plus reservoir setup. There it was proposed that this scheme

*Electronic address: jgoold@ictp.it

†Electronic address: lucas@chibebe.org

could be used in to study the Landauer principle and hence the information to energy conversion in a quantum system at the ultimate limit. In this work we exploit this scheme in order to measure the heat dissipated in elementary quantum gates at the Landauer Limit.

Quantum Heat Statistics.— Landauer’s principle states

$$\beta\langle\mathbf{Q}\rangle \geq \Delta\mathbf{S}, \quad (1)$$

where $\Delta\mathbf{S} = \mathbf{S}_i - \mathbf{S}_f$ is the change of von Neumann entropy ($\mathbf{S}(\rho) = -\text{tr}[\rho \log(\rho)]$) of the information bearing system and $\langle\mathbf{Q}\rangle$ is the average heat dissipated to the reservoir. The average heat is the first moment of a more general heat distribution $P(\mathbf{Q})$ such that $\langle\mathbf{Q}\rangle = \int P(\mathbf{Q})\mathbf{Q}d\mathbf{Q}$. Before writing down explicitly the full form of the distribution $P(\mathbf{Q})$ it is helpful to first outline the protocol.

We denote the system as \mathcal{S} and the reservoir as \mathcal{R} and assume that the initial total \mathcal{RS} state is fully uncorrelated, i.e., $\hat{\rho}_{\mathcal{RS}} = \hat{\rho}_{\mathcal{S}} \otimes \hat{\rho}_{\mathcal{R}}$. The reservoir, or non-information bearing degree of freedom, is initially in the Gibbs state $\hat{\rho}_{\mathcal{R}} = e^{-\beta\hat{H}_{\mathcal{R}}}/\mathcal{Z}_{\mathcal{R}}$, with Hamiltonian $\hat{H}_{\mathcal{R}} = \sum_m E_m|r_m\rangle\langle r_m|$, the inverse temperature β , and the partition function $\mathcal{Z}_{\mathcal{R}} = \text{tr}[e^{-\beta\hat{H}_{\mathcal{R}}}]$. The system and reservoir interact via a perfectly unitary mechanism, or computation \hat{U} . The resultant dynamics on the system or the reservoir alone is however non-unitary, which generates heat in \mathcal{R} at the expense of changing the entropy of \mathcal{S} .

Consider now the distribution of energetic changes in the reservoir after the protocol. To characterise this distribution a two point measurement scheme is required, the distribution is built by the following procedure: before the computation, the environment is projectively measured to have energy E_m with probability given by the Boltzmann factor $p_m = e^{-\beta E_m}/\mathcal{Z}_{\mathcal{R}}$, then a generally non-unitary dynamics occurs on the reservoir (and the system) and the energy is measured again with conditional probability $p_{m|n} = \text{tr}[\hat{U}|r_m\rangle\langle r_m| \otimes \hat{\rho}_{\mathcal{S}} \hat{U}^\dagger|r_n\rangle\langle r_n|]$ thus forming a distribution of heat changes defined as

$$P(\mathbf{Q}) = \sum_{mn} p_m p_{n|m} \delta(\mathbf{Q} - (E_n - E_m)). \quad (2)$$

The first moment of this distribution is shown to be $\langle\mathbf{Q}\rangle = \text{tr}[\hat{H}_{\mathcal{R}} \hat{\rho}'_{\mathcal{R}}] - \text{tr}[\hat{H}_{\mathcal{R}} \hat{\rho}_{\mathcal{R}}]$, conforming with Eq. (1). Due to the invasive nature of projective measurements, it is generally not easy to measure the heat distribution, rather we will measure the corresponding characteristic function, $\Theta(t)$, calculated by Fourier transform to be

$$\begin{aligned} \Theta(t) &= \sum_{mn} p_m p_{n|m} e^{-i(E_n - E_m)t} \\ &= \text{tr}[\hat{U} \hat{\rho}_{\mathcal{R}} \hat{v}_t^\dagger \otimes \hat{\rho}_{\mathcal{S}} \hat{U}^\dagger \hat{v}_t], \end{aligned} \quad (3)$$

where $\hat{v}_t = e^{i\hat{H}_{\mathcal{R}}t}$ is unitary transformation on \mathcal{R} . In what follows we demonstrate how the information to energy conversion of basic quantum logic gates can be studied in the quantum domain using a NMR setup.

Experimental Setup.— To measure $\Theta(t)$ we implement the circuit shown in Figure 1(a). The circuit utilises an ancillary qubit (labelled as \mathcal{A}) in superposition state $|+\rangle =$

$(|0\rangle + |1\rangle)/\sqrt{2}$. The implementation of unitary operations \hat{v}_t and \hat{v}_t^\dagger is controlled by the state of \mathcal{A} ; the operations are applied when \mathcal{A} is in state $|1\rangle$ and not applied when the state is $|0\rangle$. In between the two controlled operations, the system and the reservoir interact via \hat{U} . The expectation values for observable σ_x and σ_y on \mathcal{A} are directly related to the characteristic function $\Theta(t) = \langle\sigma_x\rangle_{\mathcal{A}(t)} - i\langle\sigma_y\rangle_{\mathcal{A}(t)}$.

We use the molecule Trifluoroiodoethylene ($\text{C}_2\text{F}_3\text{I}$), whose physical parameters are shown in Fig. 1(a). This molecule contains three fluorine atoms whose nuclei have spin-1/2, thus representing a qubit (see Supplementary Material for more details). Our system can be viewed as an ensemble of independent and identically prepared three spin-1/2 systems where the natural Ising type coupling is manifest between them [27],

$$H = \sum_j \hbar\omega_j I_z^j + \sum_{j \neq k} \hbar J_{j,k} I_z^j \otimes I_z^k + H_{rf}(t), \quad (4)$$

with $I_z^j = \sigma_z^j/2$ being the z component of the nuclear spin for system j , whose energy is $\hbar\omega_j$. The summations run over the three spins needed to perform the protocol, the ancilla \mathcal{A} , the system \mathcal{S} and the reservoir \mathcal{R} . Here $H_{rf}(t)$ is the radio-frequency control Hamiltonian which is required to perform high level control over the spins. The experiment was performed applying sequences of radio-frequency pulses suitably designed to implement the desired operations, as described in detail in the Supplementary Material.

We prepare the three fluorine qubits in the following initial product state

$$\rho_{\mathcal{ARS}} = |+\rangle\langle +| \otimes \frac{e^{-\beta\hat{H}_{\mathcal{R}}}}{\mathcal{Z}} \otimes \frac{\mathbb{1}}{2}. \quad (5)$$

The ancilla qubit is prepared in state $|+\rangle$ (initialised in $|0\rangle$ followed by a Hadamard operation). The second qubit is prepared the Gibbs thermal state for the reservoir, at the inverse temperature β . It is important to observe here that this does not correspond to the temperature of the room, being instead a controlled property of our system that we identify with the temperature of \mathcal{R} . In this way, we can vary this parameter as desired. The system is prepared in the maximally mixed state which represents the situation in which it contains one bit of information, thus functioning as a memory (details on the preparation of this state are given in the Supplementary Material). Different choices for the system would simply give a different amount of entropy variation and heat dissipated, but the validity of the Landauer’s principle is independent of this choice. A direct measurement on \mathcal{A} gives us the expectation values of σ_x and σ_y , which are shown in Figure 1(b), as a function of time, in one realisation of the circuit. We also make a measurement on \mathcal{S} to perform state tomography in order to determine the (average) change in the entropy of the system, as described in the Supplementary Material.

By computing the discrete inverse Fourier transform of the acquired data for the characteristic functions we attain the corresponding heat distributions, which are shown in Figure 2 for an example of a CNOT gate (with \mathcal{S} as the control) at different values of $\beta > 0$. The central peak at $\mathbf{Q} = 0$, in the

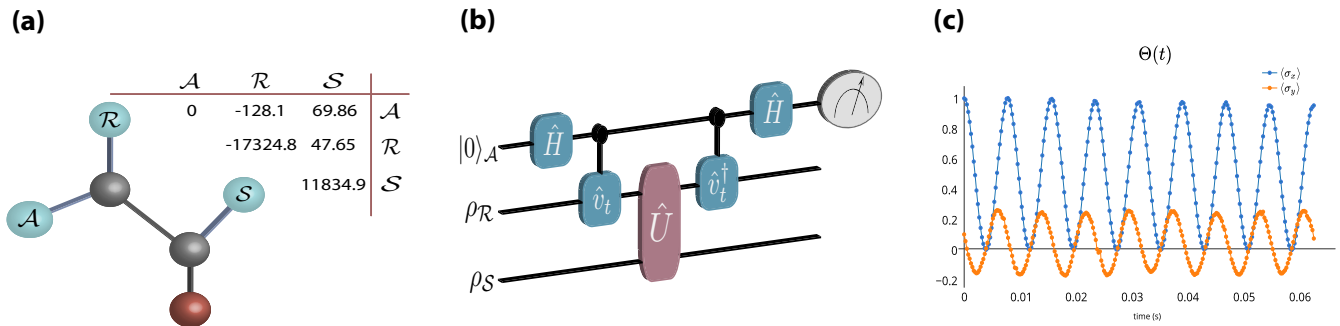


FIG. 1: **Quantum circuit.** The molecular structure of the Iodotrifluoroethylene molecule is shown in panel (a), together with its Hamiltonian parameters. The diagonal elements are the relative frequencies, with respect to the ancilla, while the off-diagonal ones are the coupling strengths (J), all of them measured in Hz. Our three qubits are the fluorine nuclei labelled as \mathcal{A} , \mathcal{R} and \mathcal{S} . As outlined in [24] by employing the ancilla system we perform the appropriate phase estimation as illustrated in panel (b). The Hadamard gates H and the controlled operations $\hat{v}_t = e^{-i\hat{H}\mathcal{R}t}$ and its Hermitian conjugate \hat{v}_t^\dagger are necessary to effectively make an interferometer [25, 26]. The purpose of this circuit is to map the heat distribution for the reservoir onto the transversal magnetisations of the ancillary system. By varying the time t of this operation the phase difference can be measured and by appropriate measurements of the ancilla the characteristic function of the distribution of heat dissipated to the environment can be reconstructed, as shown in panel (c). Further details of the experiment are presented in the Supplementary Material.

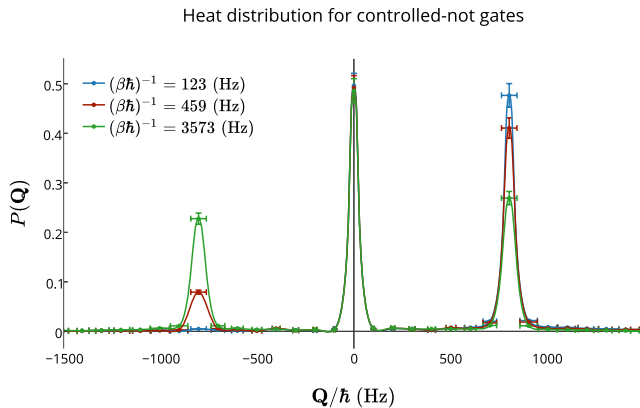


FIG. 2: **Heat distribution for CNOT gate** Shown above are the heat distributions for the CNOT gate for three different temperatures, the theoretical entropy change is $\Delta\mathbf{S} = 0$ in all cases. The three peaks represent transitions from high to low energy and vice-versa and the central peak represents the probability to dissipate no heat. The distribution becomes more asymmetric to the right as the temperature increased as transitions from high to low energy become less likely due to suppression of thermal fluctuations.

heat distributions, corresponds to the cases where the energy eigenstate does not change, while $\mathbf{Q} > 0$ means a transition from low energy state to high energy state has occurred, while $\mathbf{Q} < 0$ represents reverse situation. For this particular gate it is straightforward to see that the theoretical entropy change is $\Delta\mathbf{S} = 0$. However as is clearly shown, there are instances where $\mathbf{Q} < 0$, seemingly in violation with the Landauer principle. Reinforcing the statistical concept of the 2nd law, these events are fluctuations and the stochastic nature of the thermodynamic variables in this domain is emphasised. As we can see, although there is a probability to observe a transient *violation* of Landauer's bound, the *average* heat is greater than the entropy variation, reinforcing the view that Landauer's

principle (as well as the second law) are valid on average, but not for necessarily a single realisation of the experiment. In what follows we now use the average value to explore the heat dissipated for information processing at the ultimate limit.

Exploring the Landauer Limit.— We now change the unitary to implement a *partial swap* operation, the strength of the partial swap is varied by changing the $\mathcal{R}\mathcal{S}$ interaction. Figure 3(a) shows the average heat which is dissipated versus the theoretically computed entropy variation for increasing strength. The case of $\theta = \pi$ is a full *swap* operation which can be seen as the paradigmatic example of the erasure protocol, since the final state of \mathcal{S} is the initial state of \mathcal{R} , irrespective its initial state of \mathcal{S} . In all cases we confirm that the Landauer principle holds. The feature of the Figure 3(a) which initially strikes us is the discrepancy between experiment and theory. This difference is understood as being due to the fundamental irreversible entropy production due to the finite size environment. It has been shown by Esposito *et al* [29] that the average irreversible entropy production $\langle \Sigma \rangle$ can be computed as

$$\langle \Sigma \rangle = \beta \langle \mathbf{Q} \rangle - \Delta\mathbf{S} = \mathcal{I}(\rho'_S : \rho'_R) + \mathcal{D}(\rho'_R \| \rho_S). \quad (6)$$

where $\mathcal{I}(x : y) := \mathbf{S}(x) + \mathbf{S}(y) - \mathbf{S}(x, y)$ is the mutual information between the system and environment at the end of the computation and $\mathcal{D}(x \| y) := -\text{tr}[x \log(y)] - \mathbf{S}(x)$ is the relative entropy between the states of the environment before and after the computation. The former quantifies the correlations built and the latter the change in the state of the environment. It is straightforward to see that in the limit of weak coupling and large reservoir dimension that these terms will vanish and we recover the expected result: $\beta \langle \mathbf{Q} \rangle = \Delta\mathbf{S}$. It is important to point out that the positivity of the average entropic contribution $\langle \Sigma \rangle$ was used recently by Reeb and Wolf in order to provide finite size corrections to the Landauer bound [28]. In Figure 3(b) we plot the experimentally measured $\langle \Sigma \rangle$ right hand side of the last equation with theoretically computed quantity.

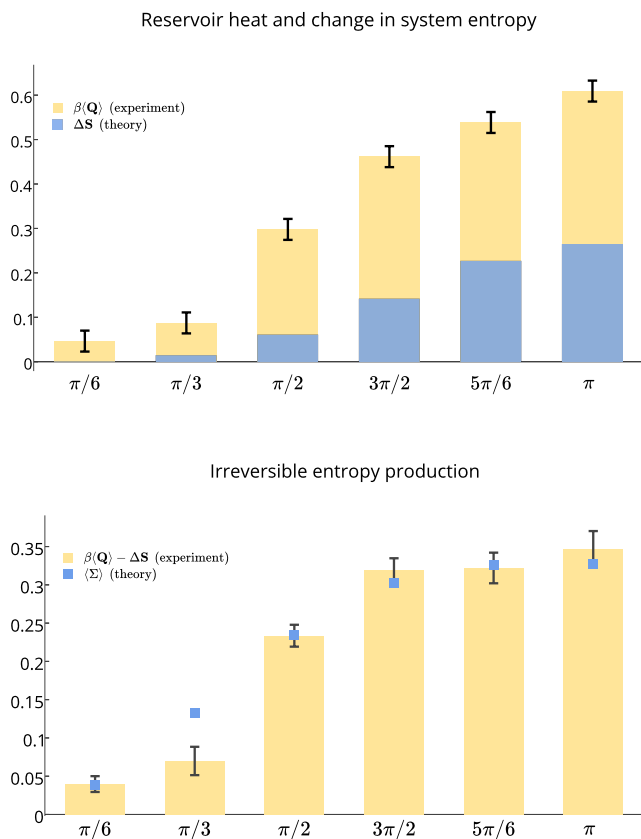


FIG. 3: **Landauer Limit for Partial Swap gate** In (a) we compare the measured average heat generated in \mathcal{R} to theoretical change in entropy of \mathcal{S} . In (b) we compare the experimentally measured gap between heat and entropy to the theoretically computed irreversible entropy production [28, 29].

The agreement between experiment and theory here confirms that we have measured the heat dissipated by an elementary quantum logic gate at the ultimate limit.

Conclusions.— In this work we have used a modified phase estimation scheme for the extraction of heat statistics from elementary quantum logic gates which were implemented in an NMR experimental setup. The experimental acquisition of the heat statistics allowed us to extract the average heat dissipated during a computation at the ultimate limit set by the Landauer’s principle. Although for the purpose of demonstration we have focused on specific gate implementations, the scheme is sufficiently general to explore entropy production in a range of gate operations and elementary circuits which are central to the theory of quantum computation. We believe that this experiment will open an avenue for further pioneering experiments on the thermodynamics of systems at the fundamental quantum limit.

-
- [1] R. Landauer. Irreversibility and heat generation in the computing process, *IBM J. Res. Dev.* **5**, 183 (1961).
- [2] C. Bennett. Logical reversibility of computation. *Int. J. Theor. Phys.* **17**, 525 (1973).
- [3] O. Penrose, *Foundations of statistical mechanics: A deductive treatment* (Pergamon, New York, 1970).
- [4] J. C. Maxwell, *The theory of heat* (Appleton, London, 1871).
- [5] W. Thompson. Kinetic theory of the dissipation of energy. **Nature**, 441 (1874).
- [6] L. Szilárd. ”Über die entropieverminderung in einem thermodynamischen system bei eingriffen intelligenter wesen. *Z. Phys.* **53**, 840 (1929).
- [7] H. S. Leff & A. R. Rex, *Maxwell’s demon 2: Entropy, Classical and Quantum information, Computing* (IOP London, 2003).
- [8] K. Manuyama, F. Nori & V. Vedral, *The Physics of Maxwells demon and information*, *Rev. Mod. Phys.* **81**, 1, (2009).
- [9] A. O. Orlov, C. S. Lent, C. C. Thorpe, G. P. Boechler & G. L. Snider. Experimental test of Landauers principle at the sub- $k_B T$ level. *Jpn. J. Appl. Phys.* **51**, 06FE10 (2012).
- [10] S. Toyabe, T. Sagawa, M. Ueda, E. Muneyuki & M. Sano. Experimental demonstration of information-to-energy conversion and validation of the generalised Jarzynski equality. *Nat. Phys.* **6**, 988, (2010).
- [11] A. Bérut, A. Arakelyan, A. Petrosyan, S. Ciliberto, R. Dillenschneider & E. Lutz. Experimental verification of Landauer’s principle linking information and thermodynamics. *Nature* **483**, 187 (2012).
- [12] J. V. Koski, V. F. Maisi. J. P. Pekola & D. V. Averin. Experimental realization of Szilard engine with a single electron. *Proc. Natl. Acad. Sci. USA* **111**, 13786 (2014).
- [13] Y. Jun, M. Gavrilov & J. Bechhoefer. High-precision test of Landauer’s principle in a feedback trap. *Phys. Rev. Lett.* **113**, 190601 (2014).
- [14] K. Sekimoto, *Stochastic energetics* (Springer, New York, 2010).
- [15] U. Seifert. Stochastic thermodynamics, fluctuation theorems and molecular machines. *Rep. Prog. Phys.* **75**, 126001 (2012).
- [16] M. Esposito, U. Harbola & S. Mukamel. Colloquium: Quantum fluctuation relations: Foundations and applications. *Rev. Mod. Phys.* **81**, 1665 (2009).
- [17] M. Campisi, P. Hänggi & P. Talkner. Nonequilibrium fluctuations, fluctuation theorems and counting statistics. *Rev. Mod. Phys.* **83**, 771 (2011).
- [18] P. Talkner, E. Lutz & P. Hänggi. Work is not an observable. *Phys. Rev. E* **75**, 050102R (2007).
- [19] R. Dorner, S. R. Clark, L. Heaney, R. Fazio, J. Goold & V. Vedral. Extracting quantum work statistics and fluctuation

theorems by single qubit interferometry. *Phys. Rev. Lett.* **110**, 230601 (2013).

- [20] L. Mazzola, G. De Chiara & M. Paternostro. Measuring the characteristic function of the work distribution. *Phys. Rev. Lett.* **110**, 230602 (2013).
- [21] T. B. Batalhão, A. M. Souza, L. Mazzola, R. Aucaise, R. S. Sarthour, I. S. Oliveira, J. Goold, G. De Chiara, M. Paternostro & R. M. Serra. Experimental reconstruction of work distribution and study of fluctuation relations in a closed quantum system. *Phys. Rev. Lett.* **113**, 140601 (2014).
- [22] M. Campisi, R. Blattmann, S. Kohler, D. Zueco & P. Hänggi. Employing circuit QED to measure nonequilibrium work fluctuations. *New J. Phys* **15**, 105028, (2013).
- [23] L. Mazzola, G. De Chiara & M. Paternostro. Detecting the work statistics through Ramsey-like interferometry. *Int. J. Quantum Inform.* **12**, 1461007 (2014).
- [24] J. Goold, U. Poschinger & K. Modi. Measuring the heat exchange of a quantum process. *Phys. Rev. E* **90**, 020101(R) (2014).
- [25] D. O. Soares-Pinto, R. Aucaise, J. Maziero, A. Gavini-Viana, R. M. Serra & L. C. Céleri, On the quantumness of correlations in nuclear magnetic resonance. *Phil. Trans. R. Soc. A* **370**, 4821 (2012).
- [26] R. Aucaise, R. M. Serra, J. G. Filgueiras, R. S. Sarthour, I. S. Oliveira & L. C. Céleri. Experimental analysis of the quantum complementarity principle. *Phys. Rev. A* **85**, 032121 (2012).
- [27] L. M. K. Vandersypen & I. L. Chuang. NMR techniques for quantum control and computation. *Rev. Mod. Phys.* **73**, 1037 (2005).
- [28] D. Reeb & M. W. Wolf. An improved Landauer principle with finite-size corrections. *New J. Phys* **16**, 103011 (2014).
- [29] M. Esposito, K. Lindenberg & C. van den Broeck. Entropy production as correlation between system and reservoir. *New J. Phys* **12** 013013 (2010).

Acknowledgements:

This work was partially supported by the COST Action MP1209. We also acknowledge financial support from CNPq, CAPES, FAPESP and FAPERJ. Financial support was also provided by Instituto Nacional de Ciência e Tecnologia de Informação Quântica.

Appendix A: The system

Our experiments were performed in a Varian 500 MHz Spectrometer and a double resonance probe-head equipped with a magnetic field gradient coil, at room temperature ($T = 300$ K). The three spin-1/2 ^{19}F nuclei of Trifluoroiodoethylene ($\text{C}_2\text{F}_3\text{I}$) molecule, dissolved in acetone D_6 (97%), were employed as our qubits. The natural Hamiltonian of our system is given by the Ising model

$$H = \sum_j \hbar\omega_j I_z^j + \sum_{j \neq k} \hbar J_{j,k} I_z^j \otimes I_z^k + H_{rf}(t), \quad (\text{A1})$$

with $I_z^j = \sigma_z^j/2$ being the nuclear spin operator in z -direction for spin j whose energy is $\hbar\omega_j$ (σ_z^j is the Pauli matrix). $H_{rf}(t) = 2\pi\nu (\sigma_x^j \cos(\omega_{rf}t) + \sigma_y^j \sin(\omega_{rf}t))$ is the radio-frequency Hamiltonian employed to perform controlled rotations on qubit j , by suitably choosing the parameters ν and ω_{rf} . The physical parameters of our molecule are shown in Fig. 4.

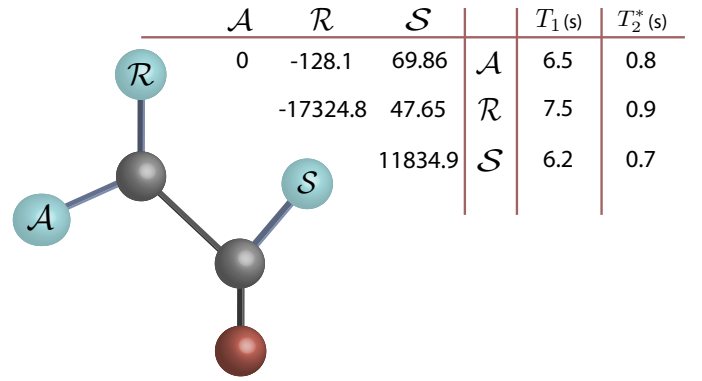


FIG. 4: **Physical parameters of the sample.** Molecular structure of the Iodotrifluoroethylene molecule, together with its Hamiltonian parameters. The diagonal elements are the relative frequencies, with respect to the ancilla ($\omega_j - \omega_{\mathcal{A}}$), while the off-diagonal ones are the coupling strengths ($J_{i,j}$). The longitudinal (T_1) and transversal (T_2^*) relaxation times are also shown. All the frequencies are measured in Hz. Our three qubits are the fluorine nuclei labelled as \mathcal{A} , \mathcal{R} and \mathcal{S} . The grey spheres represents carbon nuclei while the red one is the iodine.

Appendix B: Experimental details

Since we are studying a thermodynamic process, a definition of temperature is therefore necessary. Remembering that, in the NMR setup, the system is actually prepared in the so called pseudopure state $\rho_{NMR} = (1-\varepsilon)\mathbb{1}/8 + \varepsilon\rho$ ($\varepsilon \sim 10^{-5}$) instead of a pure state ρ [1, 2], in Fig. 5, the pulse sequence employed to prepare the initial state of our experiments is shown. The initial state of the system, before the pulse sequence, is given by the thermal on

$$\rho = I_z^{\mathcal{A}} \otimes \frac{\mathbb{1}_{\mathcal{R}}}{2} \otimes \frac{\mathbb{1}_{\mathcal{S}}}{2} + \frac{\mathbb{1}_{\mathcal{A}}}{2} \otimes I_z^{\mathcal{R}} \otimes \frac{\mathbb{1}_{\mathcal{S}}}{2} + \frac{\mathbb{1}}{2} \otimes \frac{\mathbb{1}}{2} \otimes I_z^{\mathcal{A}}$$

After the application of the pulse sequence the state changes to (note that the gradient operation is a non-unitary one)

$$\rho = \rho_{\mathcal{A}} \otimes \rho_{\mathcal{S}} \otimes \rho_{\mathcal{R}} = |+\rangle\langle+| \otimes \frac{\mathbb{1}_{\mathcal{S}}}{2} \otimes \rho_{\mathcal{R}},$$

where

$$\rho_{\mathcal{R}} = \begin{bmatrix} x & 0 \\ 0 & 1-x \end{bmatrix} \quad \text{with} \quad x = \cos^2\left(\frac{\alpha}{2}\right).$$

Comparing this with the definition of the density matrix of a system in thermal equilibrium at finite inverse temperature β ,

$$\rho_{\mathcal{R}} \equiv \frac{e^{-\beta H_{\mathcal{R}}}}{\mathcal{Z}},$$

one can obtain a relation between the temperature and the rotation angle α with the reservoir temperature

$$\beta^{-1} = \frac{2\pi\hbar J_{\mathcal{R}\mathcal{A}}}{\log\left[\tan^2\left(\frac{\alpha}{2}\right)\right]},$$

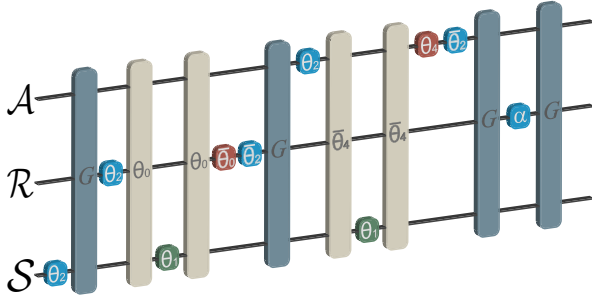


FIG. 5: **Pulse sequence for the initial state preparation.** The green, blue and red squared symbols in each line represents local rotations on the spins over the x -, y - and z -directions, respectively. There are two kinds of global operations, the darker ones represent field gradients while the lighter are free evolutions. The values of the angles inside each symbol, which characterize each operation, are given by $\theta_0 = -70.5/2^\circ$, $\theta_n = \pi/n$ for ($n > 0$) and $\bar{\theta}_n = -\theta_n$. The last rotation on the reservoir qubit, denoted by α , is used to define the temperature, as explained in the text.

From this equation we see that we can prepare states in the range $\beta^{-1} \in [0, \infty)$ by just taking the limits $\alpha \rightarrow \pi/2$ and $\alpha \rightarrow 0$, respectively. We shall proceed with the measurement of the heat distribution.

1. The unitary operations

The Hamiltonian of the system is given by is given in Eq. (A1). To perform the unitary operations U_i we employ the pulse sequence showed in Fig. 6. The main goal of this sequence is to implement a Heisenberg Hamiltonian between the reservoir and the system, given by

$$H_h = \hbar(\omega_{\mathcal{R}} - \omega_{\mathcal{A}})I_z^{\mathcal{R}} + \hbar(\omega_{\mathcal{S}} - \omega_{\mathcal{A}})I_z^{\mathcal{S}} + 2\pi\hbar J_{\mathcal{RS}} (I_x^{\mathcal{R}} \otimes I_x^{\mathcal{S}} + I_y^{\mathcal{R}} \otimes I_y^{\mathcal{S}} + I_z^{\mathcal{R}} \otimes I_z^{\mathcal{S}}) \quad (\text{B1})$$

Note that this equation is written in the ancilla rotating frame. This is the chosen reference frame for all the experiments performed here. Therefore, the effective evolution operator implemented by the pulse sequence in Fig. 6 can be written as

$$\hat{U}(\tau) = e^{-iH_h\tau/\hbar}.$$

The relation between τ and the rotation angle φ appearing in Fig. 6 is given by

$$\varphi = 2\pi J_{\mathcal{RS}}\tau,$$

with $J_{\mathcal{RS}} = 47.65\text{Hz}$ in our experiment (see Fig. 4). We then vary τ from $\tau = 0$ (the identity operation) to $\tau = 1/2J_{\mathcal{RS}}$ which implements the complete SWAP. It is important to note here that undesired rotations—the first two terms in Eq. (B1)—around the z axis are present in our system, but fortunately they can be compensated using the techniques described in Ref. [3].

The \hat{v}_t operation is implemented by a free evolution during a time $t/2$ followed by a π pulse in the x -direction on the

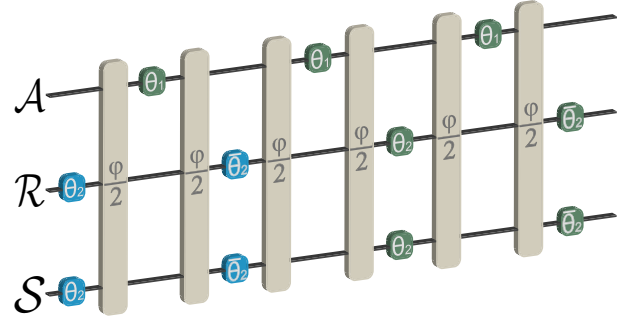


FIG. 6: **Pulse sequence to implement $\hat{U}(\tau)$.** The labels here follow the same pattern of the ones in Fig. 5. To implement different global unitaries we need to change the value of φ , as explained in the text. When $\varphi = 0$ we have the identity operation (on the system and reservoir). $\varphi = \pi$ and $\varphi = \pi/2$ implements the SWAP and the square root of the SWAP operations, respectively.

system qubit and another $t/2$ free evolution. For the $\hat{v}_t^\dagger(t)$ we apply a $\pi/2$ pulse in the y -direction on the ancilla qubit, a $t/2$ free evolution, a π pulse in the x -direction on the system qubit, followed by another $t/2$ free evolution.

2. The CNOT operation

The pulse sequence for the CNOT operation is

$$R_x^{\mathcal{R}}\left(\frac{\pi}{2}\right)U\left(\frac{\pi}{2}\right)R_x^{\mathcal{A}}(\pi)U\left(\frac{\pi}{2}\right)R_y^{\mathcal{R}}\left(\frac{\pi}{2}\right),$$

where $R_k^i(\alpha)$ is a rotation on the i -th qubit about direction k by an angle α . We performed several experiments by varying the temperature of the reservoir and the results are shown in Table I. As we can see, the measured irreversible entropy production and heat dissipated are equal to each other, confirming Landauer's principle as stated in Eq. (6) of the main text.

3. Error analysis

To implement single-spin operations, we exploit standard Isech shaped pulses as well as numerically optimized GRAPE pulses [4]. The GRAPE pulses are optimized to be robust to radio frequency (r.f.) inhomogeneities and chemical shift variations. Two qubit operations were implemented by interleaving free evolutions periods with selective π pulses, introduced into the sequences in order to refocalize unwanted couplings during the gate.

For combining all operations into a single pulse sequence we have used the techniques described in [3, 4] for Ising coupled system. We built a computer program, similar to the NMR quantum compiler used in the 7 qubits NMR experiments [5–7]. This program loads the information about the internal Hamiltonian and the desired unitary transformation from simple predefined building blocks and combine all blocks together ensuring that the errors in the building blocks

$(\beta\hbar)^{-1}$ (Hz)	$\langle\Sigma\rangle$ (exp.)	$\beta\langle\mathbf{Q}\rangle$ (exp.)	Γ (theo.)
123	3.2(2)	3.3(2)	3.3
185	2.1(1)	2.1(1)	2.1
227	1.64(8)	1.66(8)	1.67
274	1.30(6)	1.32(7)	1.32
324	1.03(5)	1.04(5)	1.05
383	0.80(4)	0.82(4)	0.82
458	0.61(3)	0.62(3)	0.63
550	0.45(2)	0.45(2)	0.46
678	0.31(2)	0.31(2)	0.32
862	0.20(1)	0.20(1)	0.20
1168	0.113(6)	0.114(6)	0.114
1775	0.050(2)	0.052(3)	0.051
3573	0.0128(6)	0.0171(9)	0.0126

TABLE I: **CNOT experiments.** Measurement of average heat dissipated for the controlled-not gate for several temperatures. For this case, the theory predicts that $\Delta\mathbf{S} = 0$ (value also obtained experimentally) and the heat dissipated maybe expressed (see text) as $\langle\Sigma\rangle = I(\rho'_R : \rho'_S) + D(\rho'_R || \rho_S) \equiv \beta\langle\mathbf{Q}\rangle$ with $\rho' = \hat{U}\rho\hat{U}^\dagger$ and \hat{U} is the CNOT operation (see main text). As we can see from the data, the Irreversible entropy production due to the implementation of the CNOT gate perfectly matches the heat dissipated, both agreeing with the theoretical prediction. The number in parenthesis are the experimental errors, i.e. $3.2(2) = 3.2 \pm 0.2$.

do not propagate as the sequence progresses. The program is capable of minimizing the effects of finite pulse-width and off-resonance errors as well as unwanted coupling evolutions.

Errors in the pulses — There are two main error sources here, the signal acquisition (reading) and the duration of each pulse (which is not exactly equal to the planned one). Both these errors were extensively studied in [8]. Assuming that both errors are independent, it was estimated the combined result of $\approx 1\%$ on the magnetization of the spins. However, in order to work with mononuclear systems shaped pulses are necessary. This improves the precision of the required operations, but increases the duration of the pulses, which contributes to the decoherences processes (see bellow).

Errors in the entropies — The experimental procedure to determine the entropies requires a smaller amount of pulses (due to the lack of the \hat{v}_t operation, which also makes it faster). Therefore, the errors in the entropies are much smaller than the ones in the heat distribution.

The experimental states were reconstructed by quantum state tomography [9] and the fidelity obtained was, in the worst case, 5%. The precision of the whole process can be estimated by comparing the fidelities of the measured density

matrices and the theoretically calculated ones. For the tested cases we have determined that it was between 2% (fidelity of ~ 0.98) and 7% (fidelity of ~ 0.93), at most. From this, it was possible to estimate, through standard statistical methods, the error bars for the entropies determined on the experiments reported on this paper.

Errors in the heat — The errors in the heat distribution are caused mainly by two sources. The first one is decoherence, which is discussed bellow. The second one, much more seriously because we cannot correct it, is due to the numerical computation of the inverse Fourier transform of the acquired data. For the determination of the characteristic function only one qubit is measured, which is equivalent to the measurement of the nuclear spin magnetization. This measurement can be achieved with high precision in NMR systems. The error bar for the experimental determination of the average heat was estimated from the standard deviation of the measured points for the characteristic function. Then, we have used standard error propagation for calculating the error bars. In some cases, the oscillations of characteristic function over time are small when compared with the average of $\Theta(t)$, over time. When this happens we have a larger uncertainty.

Decoherence — The data acquisition time for the SWAP case varies appreciably, reaching around 150 ms. This is relatively long when compared with the transversal relaxation time for our sample (see Fig. 4). Therefore, the signal lost due to decoherence is considerable and we need to take it into account. To do this we performed numerical simulations of the experiment considering the action of local phase damping channels, which is a very good model for the kind of noise we have [10]. This noise will cause an exponential decay in the oscillations of the magnetization, whose inverse Fourier transform will give us the heat distribution. An excellent agreement between our numerical simulations and the experimental data was then observed. The net effect was to produce a constant shift in the data both for the heat distribution and for the entropies. We then employed this analysis to correct the final data for signal loss, leading us to the results presented in the main text. The controlled-not gates are much faster and the signal loss was not significant. The spin-lattice relaxation, which is characterized by T_1 , causes no appreciable effect during the experiment for both gates.

Therefore, the high level of precision of our setup guarantees that the experimentally implemented operations (CNOT and SWAP gates) are very close to the ideal ones, as also confirmed by the excellent agreement between experiment and theory observed in this work.

[1] N. Gershenfeld & I. Chuang. Bulk Spin-Resonance Quantum Computation. *Science* **275**, 350 (1997)
[2] D. Cory, A. Fahmy & T. Havel. Ensemble quantum computing by NMR spectroscopy. *Proc. Natl. Acad. Sci. USA* **94**, 1634 (1997).
[3] C. A. Ryan, C. Negrevergne, M. Laforest, E. Knill & R. Laflamme. Liquid-state nuclear magnetic resonance as a testbed

for developing quantum control methods. *Phys. Rev. A* **78**, 012328 (2008).
[4] M. D. Bowdrey, J. A. Jones, E. Knill & R. Laflamme. Compiling gate networks on an Ising quantum computer. *Phys. Rev. A* **72**, 032315 (2005)
[5] E. Knill, R. Laflamme, R. Martinez & C.-H. Tseng. An algorithmic benchmark for quantum information processing. *Nature*

- 404**, 368 (2000)
- [6] A. M. Souza, J. Zhang, C. A. Ryan & R. Laflamme. Experimental magic state distillation for fault-tolerant quantum computing. *Nature Communications* **2**, 169 (2011)
- [7] J. Zhang, M.-H. Yung, R. Laflamme, A. Aspuru-Guzik & J. Baugh. Digital quantum simulation of the statistical mechanics of a frustrated magnet. *Nature Communications* **3**, 880 (2012)
- [8] C. Raitz, A. M. Souza, R. Aucaise, R. S. Sarthour & I. S. Oliveira. Experimental implementation of a nonthermalizing quantum thermometer. *Quantum Inf. Process* to appear.
- [9] I. S. Oliveira, T. J. Bonagamba, R. S. Sarthour, J. C. C. Freitas & R. R. deAzevedo, *NMR Quantum Information Processing* (Elsevier, Amsterdam, 2007).
- [10] M. A. Nielsen & I. L. Chuang *Quantum Computation and Quantum Information* (Cambridge University Press, January, 2011)